FLOW SIMULATION AROUND A REALISTIC FIGHTER AIRPLANE CONFIGURATION

Torsten Berglind
The Aeronautical Research Institute of Sweden (FFA)
Stockholm, Sweden

Abstract

The concept of patched C^1-continuous multiblock grids is applied to the flow region around the new Swedish fighter airplane, JAS 39 Gripen. The volume grid is generated, block by block, using transfinite interpolation. The Euler equations are integrated numerically by a centered finite volume method using an explicit Runge-Kutta scheme. Transonic flow cases are computed and the solutions demonstrate that the grid resolves all relevant flow features. The effect of different mass flux ratios at the air intake on the global solution is investigated. Also the problem of proper boundary condition on the subsonic outflow boundary at the air intake is addressed.

1. Introduction

The demand for flow computations around complex geometries has propelled the development of several numerical techniques in CFD. A variety of different kinds of computational grids have been advocated, but today two main choices can be discerned, unstructered grids or patched multiblock grids. In this work, the concept of patched C^1-continuous multiblock grids is applied to the flow region around the Swedish fighter airplane, JAS 39 Gripen.

The process of decomposing the physical space into blocks can be automatized to various extents. British Aerospace[1] has developed a grid generation system that automatically generates a multiblock topology from information of desired kinds of grids about each component. Such systems lead to an enormous amount of blocks, and the advantage in computational efficiency compared to unstructered grids can be questioned. General Dynamics has for their grid generation system[2] instead pursued interactive visual tools to facilitate the topology generation. The procedure described herein, requires that the user entirely specifies the topology. It is thereby possible to take all the intricate considerations involved with multiblock grid generation into account.

*This work is sponsored by the Defence Material Administration of Sweden, Air Material Department, Stockholm.

Grid generation is a compromise between the main goal, to resolve flow gradients as efficiently as possible, and at the same time to avoid undesired features, such as highly skewed grid cells, slope discontinuities and sudden changes in grid spacing. Some of the undesired grid features are not possible to avoid due to geometrical restrictions on the configuration surface. It is in those cases important to limit the irregularities to a region as small as possible. Also mapping singularities contribute to larger truncation errors, but are in many cases useful means to accomplish efficient grid point distributions. It is in this context important to keep in mind that the truncation errors depend on both the grid defects and the flow gradients. The efficiency of a grid can therefore be estimated first after computations of several flow cases.

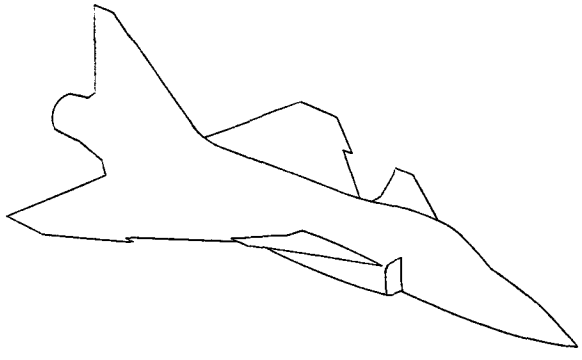

Figure 1. The JAS 39 Gripen configuration.

2. Choice of topology

The choice of topology around a complex configuration is crucial for the amount of effort required to generate the grid. By a proper choice of topology, it is usually possible to avoid regions with highly skewed grid cells. The JAS configuration consists of fuselage, canard, sawtooth delta wing, vertical fin and side mounted inlets as depicted in Figure 1. The trailing edge of the canard and the leading edge of the delta wing are partly overlapping each other in a vertical view. This can be avoided by regarding the fillet of the delta wing as a part of the

fuselage. The grid in the region between the canard and the delta wing is cumbersome to generate since the grid is required to conform to all wing edges.

Conventional multiblock topologies around airplane configurations often apply H-grids (slits) around the wing parts. For wings with round leading edges, H-grid entails very skewed grid cells at the leading edge, which is inappropriate since this is a region with high flow gradients. An alternative idea with an interior block which only covers the inner delta wing region and its wake, is presented by Eriksson[3]. One of the block faces degenerates to a singular line on the configuration surface, extending from the root chord of the delta wing to the symmetry plane. This topology implies a better resolution of the leading edge, especially where the maximum nose radius is located, close to the root chord.

In Eriksson's case, of an experimental fighter aircraft, grid lines running lengthwise on the forebody are swept outside the interior region. For the JAS configuration, the trailing edge of the canard is located very closely to the root chord of the delta wing and furthermore, the sweep angle for the delta wing is smaller than for the experimental fighter. If the same topology concept is applied to the JAS configuration, a region with highly skewed grid cells behind the rear tip of the canard appears, Figure 2a. A better choice in this case is to bend the grid lines from the lengthwise direction on the forebody into the interior region towards the symmetry plane, Fig 2b. To accomplish a smooth change from the lengthwise to the crosswise direction, a wedge shaped block is inserted in front of the leading edge. The concave corner in front of the air intake can be visually eliminated by applying a specific block, attached to the contour of the air intake and extended to the nose.

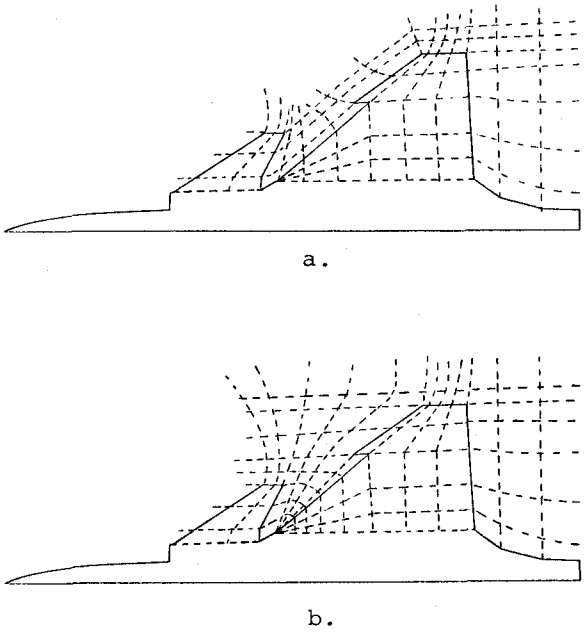

Figure 2. Alternative topologies for the canard/delta wing region.

Previous considerations formed the basis for the decomposition of the physical space into blocks. The flow solver requires that the interior of each block in terms of computational procedure is completely homogeneous, i.e. it must not contain slits or mapping singularities. Furthermore, the flow solver allows block faces with mixed boundary conditions. The decomposition of the physical space into such blocks led to a multiblock topology with eight blocks, as shown in Figure 3. This topology eliminates problems with grid skewness and automatically gives a good resolution of the region in the vicinity of the configuration.

3. Surface grid generation

The surfaces of the components are described by assemblies of cross sections. The represention of cross sections is normalized, such that each cross section contains the same number of points, distributed at the same relative accumulated chord lengths. The defined network forms the input to a parametric surface description by bicubic splines[4]. The surface parameters u and v define coordinates across and along the cross sections, respectively. The surface of each component is partitioned into smooth patches, topologically equivalent with quadrilaterals.

The grid on each surface patch is thereafter generated by distributing grid points along constant u- and v-values. This implies that the coordinate directions of the surface grid will be aligned with the directions of the surface parameters. A reorientation of cross sections is done in regions where the parameter directions did not agree with the intended grid line directions.

In cases where meeting boundary curves of two contiguous patches are not aligned, the slope discontinuity will propagate along the common boundary curve. These slope discontinuities are smoothed out by moving grid points on parametric spline curves through the original grid. The adjusted grid points will thereby automatically conform to the original surface. The slope discontinuity at these boundaries can, as shown in Figure 4, be limited to small regions. The surface grid is generated patch by patch until the whole configuration is covered, Figure 5.

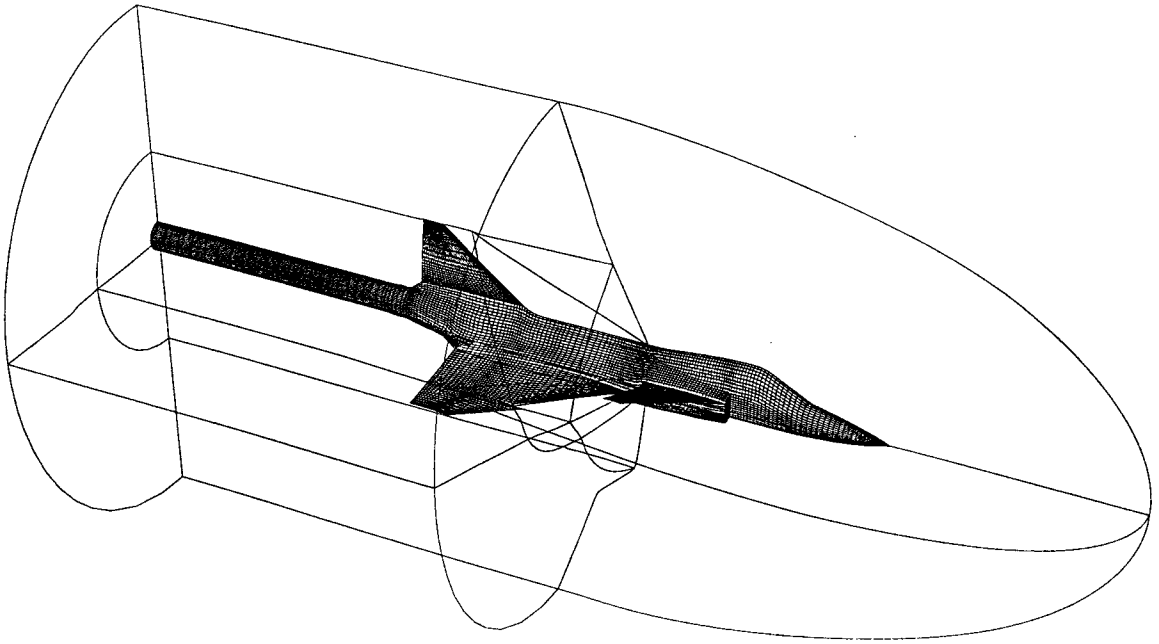

Figure 3. A wire frame model of the block decomposition.

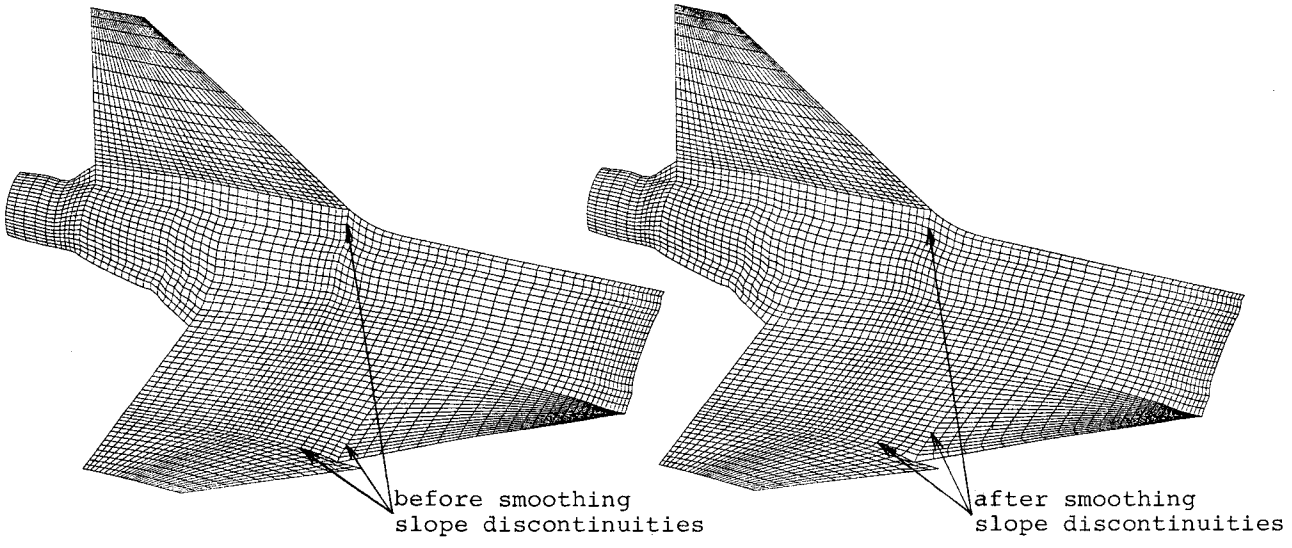

Figure 4. Before and after smoothing of slope discontinuities at the configuration surface.

5. Volume grid generation

Transfinite interpolation is a technique for multivariate interpolation that can be used for grid generation[5,6,7]. The grid is generated by either Lagrange or Hermite interpolation on several control surfaces. Hermite interpolation allows control of the orientation of grid lines, i.e. boundary orthogonality and slope continuity across block interfaces can be achieved explicitly. However a large number of interpolation conditions lead to complex blending functions and to poor control of grid lines. Particularly Hermite interpolation in concave regions has a tendency to produce grid line crossovers.

The concept used in this work is to apply a simple form of transfinite interpolation and subsequently to smooth slope discontinuities at block interfaces. It is not necessary to impose strict orthogonality at solid walls, but the accuracy deteriorates if the departure from orthogonality is too large. In our case the Euler equations are solved and orthogonality at solid walls is therefore less important than if the Navier-Stokes equations were to be solved. The volume grid is generated with interpolation conditions only on the six bounding faces of each block. The procedure can be written in a recursive form,

$$
\begin{aligned}
f^{**}(u,v,w) &= \sum_{i=1}^{2} \alpha_i(u) \cdot g(u_i,v,w) \\
f^{*}(u,v,w) &= f^{**}(u,v,w) + \\
&\quad \sum_{j=1}^{2} \beta_j(v) \cdot (g(u,v_j,w) - f^{**}(u,v_j,w)) \\
f(u,v,w) &= f^{*}(u,v,w) + \\
&\quad \sum_{k=1}^{2} \gamma_k(w) \cdot (g(u,v_k,w) - f^{*}(u,v_k,w))
\end{aligned}
\tag{1}
$$

where f^{**}, f^{*} and f are the interpolated functions after each interpolation step, and u,v and w are the curvilinear directions defined as normalized accumulated arc-lengths. The blending functions α_i, β_j and γ_k are chosen to be linear.

$$
\begin{aligned}
\alpha_1(u) &= 1-u \quad \alpha_2(u) = u \\
\beta_1(v) &= 1-v \quad \beta_2(v) = v \\
\gamma_1(w) &= 1-w \quad \gamma_2(w) = w
\end{aligned}
\tag{2}
$$

For each block, grids on all bounding block faces have to be generated in advance. Surface grids on block faces other than at the configuration surface are generated by transfinite interpolation on point distributions on boundary curves. Interfaces between these grid surfaces have been smoothed out by an algebraic technique. The slope discontinuities have preferably been smoothed out at the boundaries before the volume grid generation , since these otherwise propagate into the interior domain. All eight blocks of the topology are generated with the same technique. The resulting volume grid is shown in Figure 6.

6. Numerical Method

The numerical method is a finite volume scheme derived by applying the constant stagnation enthalpy Euler model in integral form to grid cells of hexahedronal shape[8]. The resulting semi-discrete scheme becomes,

$$
\begin{aligned}
\frac{\partial \vec{Q}}{\partial t} VOL_{i,j,k} + \vec{FI}_{i+\frac{1}{2},j,k} - \vec{FI}_{i-\frac{1}{2},j,k} + \vec{FJ}_{i,j+\frac{1}{2},k} - \\
\vec{FJ}_{i,j-\frac{1}{2},k} + \vec{FK}_{i,j,k+\frac{1}{2}} - \vec{FK}_{i,j,k-\frac{1}{2}} = 0
\end{aligned}
\tag{3}
$$

where $\vec{Q}$ denotes the flow state vector containing density and the momentum components and $\vec{FI}$,$\vec{FJ}$ and $\vec{FK}$ are the integrated fluxes in the curvilinear coordinate system associated with the i-, j-, k-indices. The non-integer indices refer to cell surface centers whereas integer indices refer to cell centers.

An explicit one-step four-stage time integration scheme that is first order accurate in time is used to integrate (3) in time[9]. Since only steady solutions are of interest, local time steps are used to accelerate the convergence to steady state. The artificial viscosity model uses a combination of a variable coefficient second-order difference operator and a constant coefficient fourth-order difference operator.

At solid walls, the wall pressure is extrapolated linearly from the interior domain. At the inflow-outflow boundaries characteristic boundary conditions[10] in their simplest form are applied. Interface grid cells are treated as interior grid cells even-though C^1-continuity could not be enforced in some small regions at configuration edges and at mapping singularities. The accuracy in these regions is consequently of less than second order. Boundary conditions for the artificial difference operators are implemented according to reference[11].

The flow at the air intake is subsonic, which means that one characteristic variable propagates into the computational domain[10], i. e. one boundary condition should be applied, Figure 7.

Since in our case, the mass flow rate $\dot{m}$ is known, a natural choice is to specify the velocity compo-

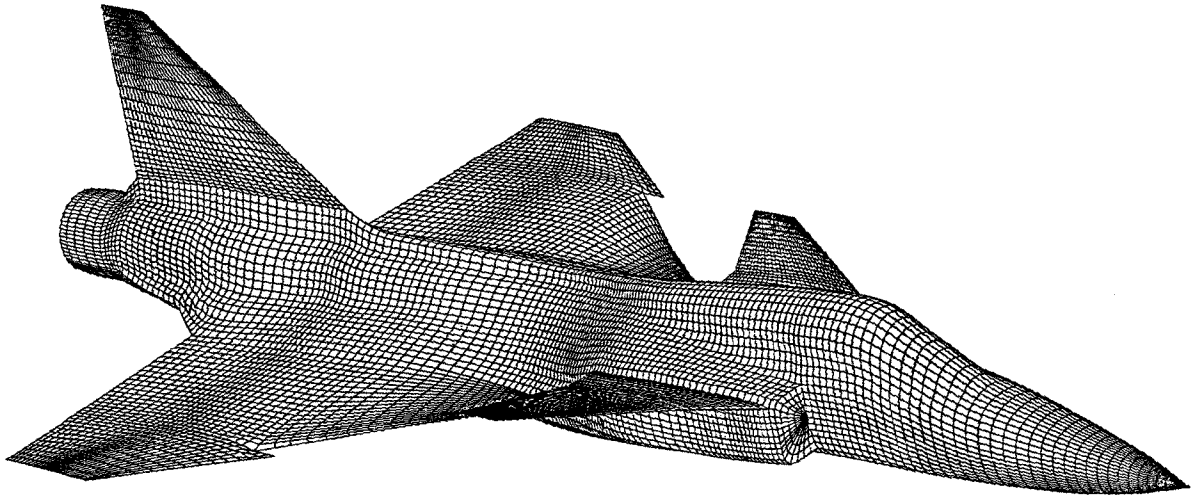

Figure 5. Oblique view of the surface grid.

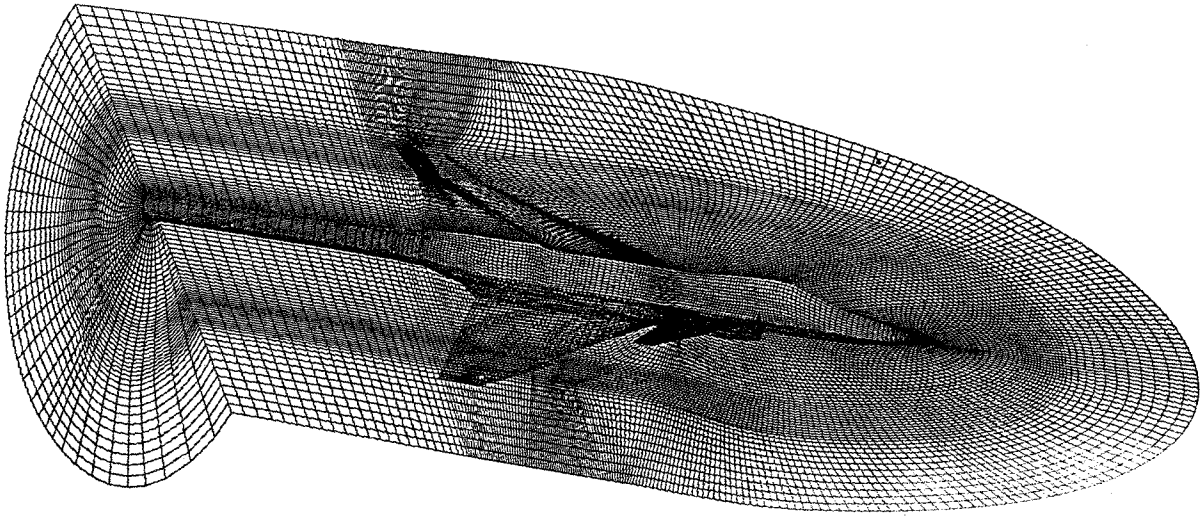

Figure 6. Oblique view of the volume grid.

nent normal to the outflow surface, here the u-component as depicted in Figure 8.

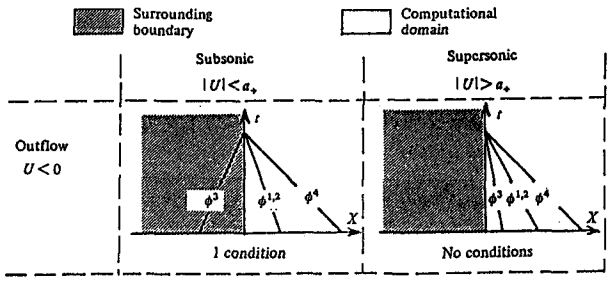

Figure 7. The number of boundary conditions at outflow based on the ingoing characteristic variables $\phi^m, m=1,\ldots,4$[11].

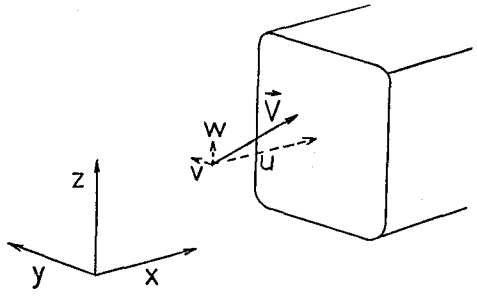

Fig 8. The outflow boundary at the air intake.

$$\dot{m} \equiv \int_A \rho(y,z) \cdot u(y,z) \cdot dydz = C_A \cdot \rho_\infty \cdot V_\infty \cdot A \qquad (4)$$

ρ is the density and C_A is the inlet mass flux ratio and A the area. We make the following ansatz for the velocity u(y,z)

$$u(y,z) \equiv u_0 \cdot \psi(y,z) \qquad (5)$$

where u_0 is a constant and ψ is a shape function of the velocity profile. The constant u_0 can now be evaluated from (4) and (5). In our case, the velocity profile is assumed to be uniform. By using zero order extrapolation of the characteristic variables pointing out of the computational domain as numerical boundary conditions, also the semi-discrete problem is well posed[12].

7. Computer Implementation

The flow computations are performed on the CRAY X-MP/48 at Saab-Scania in Linköping. Due to the limited core memory on this computer (8 Megawords), the solid state disk device SSD had to be utilized to a large extent. This meant that the original code had to be somewhat modified. The vectorization of the code was done by the Fortran compiler.

The general purpose multiblock flow solver MESC1[13] allows, as previously mentioned, mixed boundary conditions on block faces. Such a block face has to be partitioned in the computational domain into rectangular patches. A flowchart of the entire multiblock structure and boundary conditions in the computational domain is shown in Figure 9.

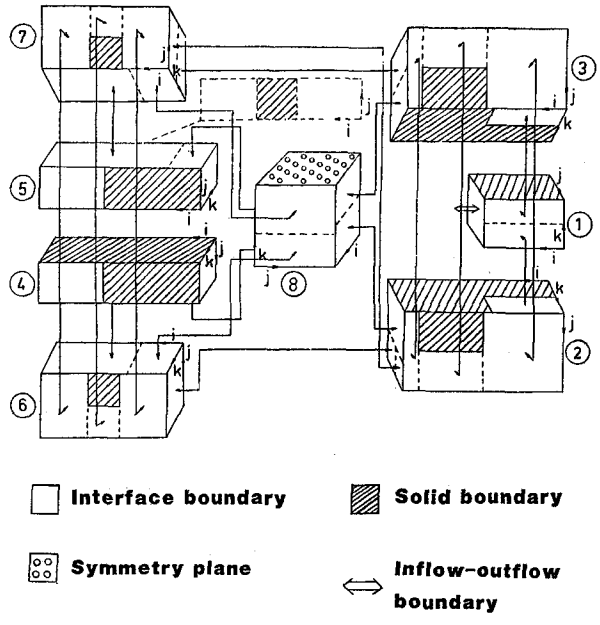

Figure 9. A flow chart of the block structure in the computational space.

8. Computational Results

Transonic flow cases are computed at the free stream Mach number 0.95 for 0.0°, 3.2° and 6.4° angles of attack. The mass flux ratio at the throat of the inlet nozzle is 0.7. The computations have been carried out for two grid sizes, 68 232 and 298 704 grid cells. Initially, solutions with all flow variables at the air intake extrapolated, are computed. These solutions are subsequently used as initial solutions for the computations with a constraint on the mass flow rate through the air intake.

Mach contours on the configuration surface at $\alpha = 0.0°$ and $6.4°$ are shown in Figures 10 and 11. Extrapolation of flow variables corresponds to a higher mass flux ratio at the air intake than 0.7. The flow solutions with the lower mass flux ratio show that a zone of slow air is forming in front of inlet to the air intake. In the region behind the inlet, a complex pattern of separation bubbles appear. Further downstream and a sharp gradient between the faster air on the delta wing and the slower air on the afterbody can be seen. The effects of lower mass flux ratio at the air intake can be clearly seen on the fuselage, whereas the effects on the canard and delta wing are small. At $\alpha = 6.4°$ local shock waves on the upper sides of both canard and delta wing appear.

The pressure measurements are performed for a configuration with the same forebody but a slightly modified afterbody and "similar" wing geometries. Comparison of measured and computed wall pressure coefficient in a position front of of the air intake is shown in Table 1. It is clear that solutions with constraint on the mass flow, compared with solutions with extrapolation of the flow variables, as expected, agree much better with the measured pressures. The good prediction of the pressure in front of the air intake, indicates a proper treatment of the outflow boundary condition at the air intake.

α	0.0°	3.2°	6.4°
C_{pm}	0.300	0.320	0.342
C_{p1}	−0.008	− 0.003	− 0.009
C_{p2}	0.325	0.325	0.327

Table 1. Comparisons of the wall pressure coefficient in front of the air intake. C_{pm} is the measured value, C_{p1} and C_{p2} are the values computed with extrapolation and with constraint on the mass flow rate, respectively.

Three component balance measurements are performed for the same configuration with tip mounted missiles. The deviation between computed and measured C_L and C_D values can be seen in Table 2. The prediction of C_L is fairly good whereas the prediction of C_D ,as usually with Euler solutions, is less good.

α	0.0°	3.2°	6.4°
ΔC_L	0.0062	0.0093	0.0182
ΔC_D	0.0128	0.0210	0.0500

Table 2. The differens betweeen measured and computed C_L an C_D values.

9. Conclusions

The computational results demonstrate that the flow solver MESC1 in conjunction with the multiblock grid system is able to capture the complex flow phenomena around the JAS 39 Gripen configuration. The few measured data accessible, confirm the computational results. The example shows that it is possible to generate efficient multiblock grids with a relatively small number of blocks around complex configurations. The mass flux ratio at the air intake is shown to have a significant impact on the global solution.

10. Acknowledgement

The author would like to thank Johan Sellström at Control Data for help to modify the geometry definition and Jan Nordström at FFA for help to formulate proper boundary conditions at the air intake.

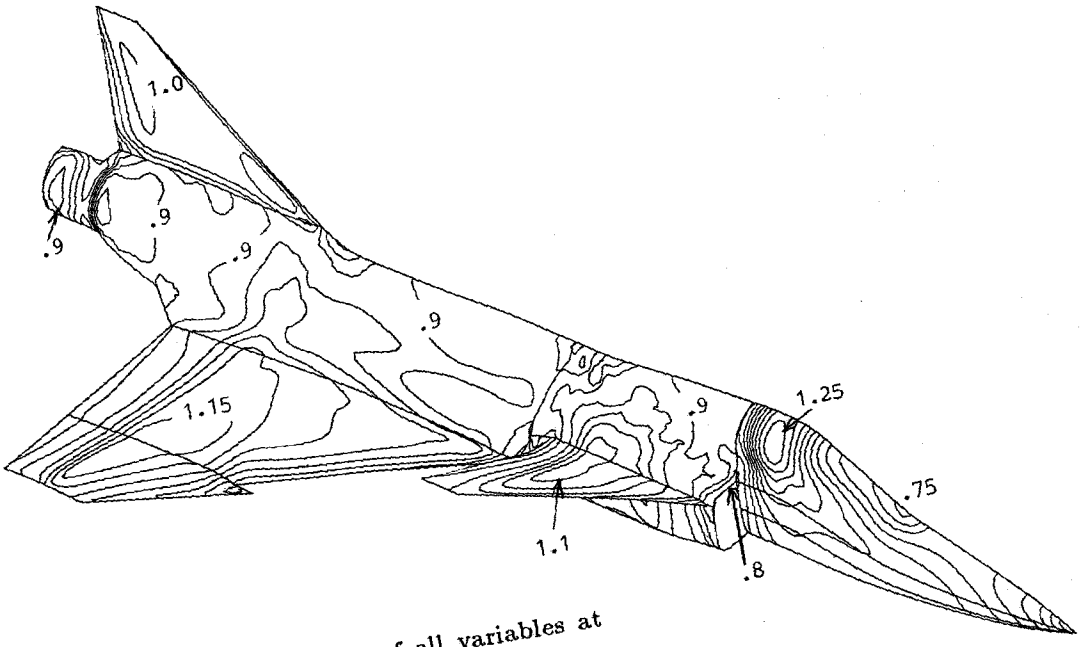

a. Solution with extrapolation of all variables at the air intake.

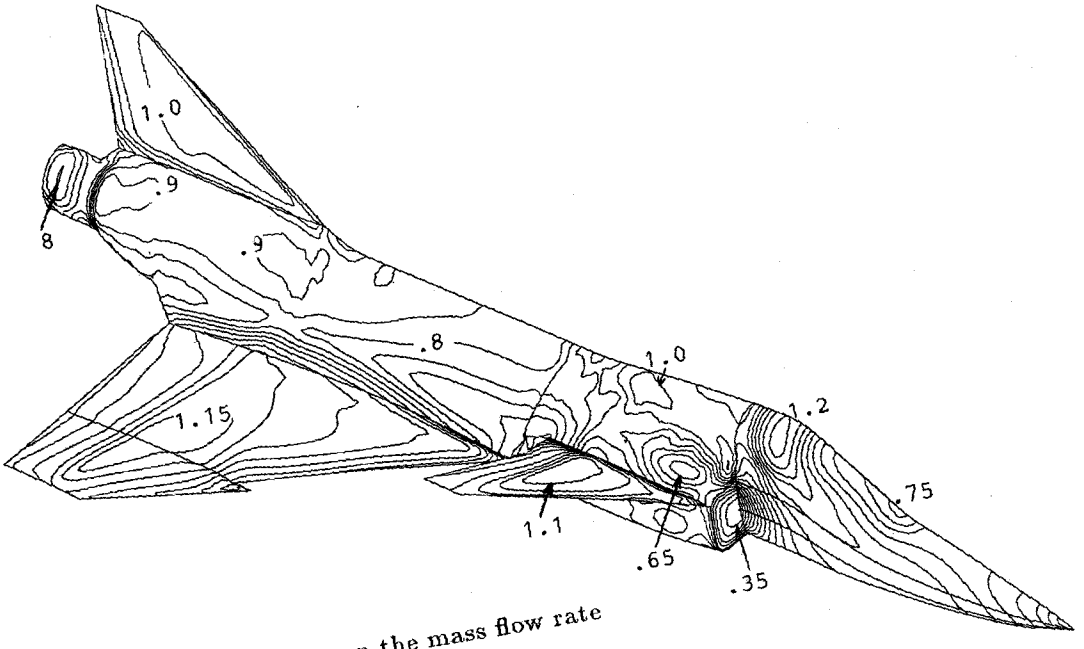

b. Solution with a constraint on the mass flow rate through the air intake.

Figure 10. Mach contours on the configuration surface, M_∞=0.95 and $\alpha = 0.0°$, $\Delta M = 0.05$.

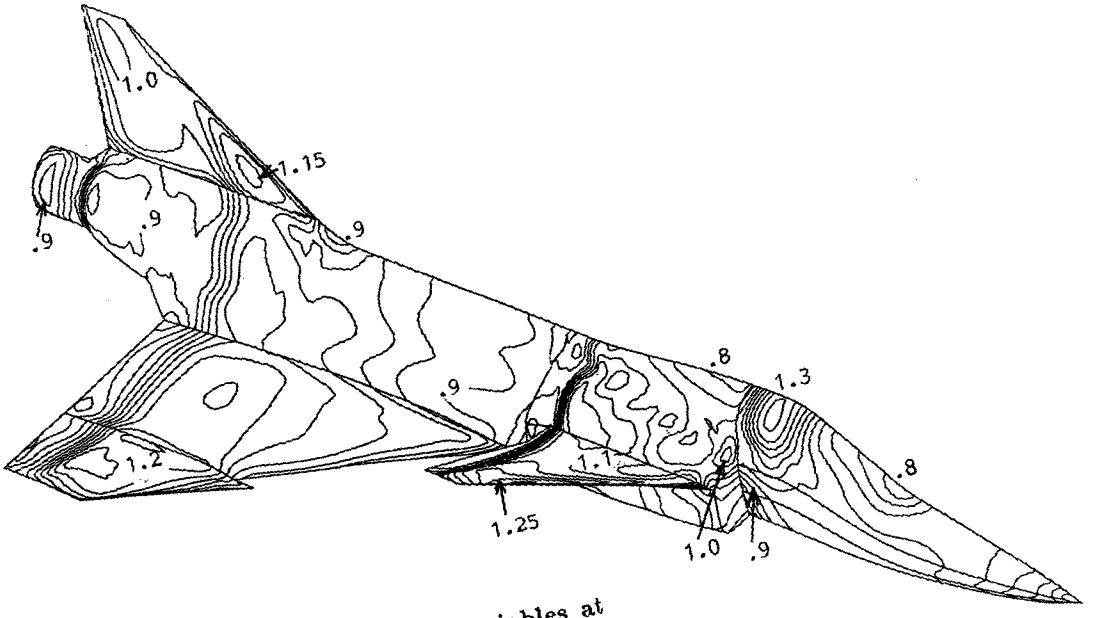

a. Solution with extrapolation of all variables at the air intake.

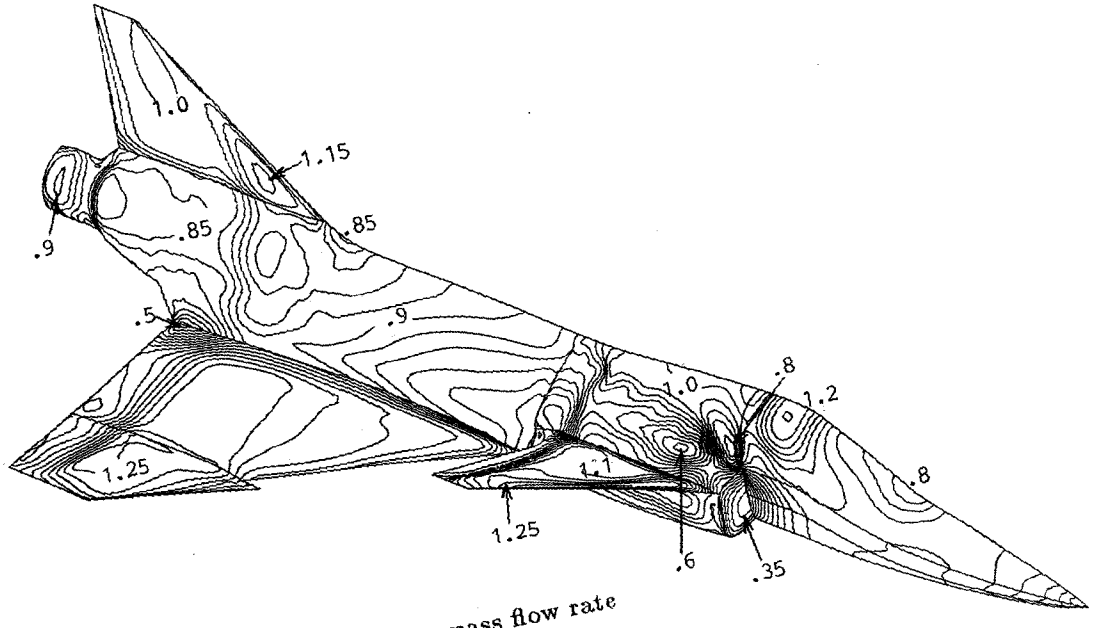

b. Solution with a constraint on the mass flow rate through the air intake.

Figure 11. Mach contours on the configuration surface, M_∞=0.95 and $\alpha = 6.4°$, $\Delta M = 0.05$.

11. References

1. Allwright S. E. - "Multiblock Techniques for Transonic Flow Computations about Complex A/C Configurations", Proceedings of the AGARD Specialists' meeting: Applications of Mesh Generation to Complex 3-D Configurations, Loen, Norway 1989.

2. Steinbrenner, J. P. Chawner J. R. and Fouts C. L., "A structured Approach to Interactive Multiple Block Grid Generation ", Proceedings of the AGARD Specialists' meeting: Applications of Mesh Generation to Complex 3-D Configurations, Loen, Norway 1989.

3. Eriksson L.E. - "Flow Solution on a Dual Block Grid around an Airplane", Computer Methods in Applied Mechanics and Engineering 64 (1987) 79-93, North Holland.

4. De Boor C., "Bicubic Spline Interpolation", J. Math. Phys. 41,212-218.

5. Eriksson, L.E., "Three-Dimensional Spline-Generat-ed Coordinate Transformations for Grids around Wing-Body Configurations", Numerical Grid Generation Techniques, NASA CP 2166, 1980.

6. Eriksson, L.E., "Generation of Boundary-Confor-ming Grids around Wing-Body Configurations Using Transfinite Interpolation", AIAA Journal, Vol. 20, 1982, pp. 1313-1320.

7. Berglind T., "The Generation of Continuous multi-block Grids around Car Configurations above a Flat Ground Plane Using Transfinite Interpolation", Proceedings of the International Conferens on Numerical Grid Generation in Computational Fluid Dynamics, Landshut, W. Germany, 14-17th July, 1986.

8. Rizzi A. and Eriksson L-E., "Computation of Flow around Wings Based on the Euler Equations", J. Fluid. Mech., Vol. 148, pp 45-71, 1985.

9. Eliasson P., "Navier-Stokes Solutions for Laminar Incompressible Flow over a Backward Facing Step", FFA TN 1987-50.

10. Enqvist B. and Madja A., "Absorbing boundary conditions for the numerical simulation of vawes. Math. Comp. 31, 629-651.

11. Eriksson L.E., "Boundary Conditions for Artificial Dissipation Operators", FFA TN 1984-53, Stockholm 1984.

12. Nordström J., "The Influence of Open Boundary Conditions on the Convergence to Steady State for the Navier-Stokes Equations", J. Comp. Phys., Vol. 85, No. 1, November 1989.

13. Berglind T., "Multi-block Euler Method Using Pat-ched Grids", Proceedings of the Second International Symposium on Domain Decomposition Methods, UCLA, Los Angeles, USA, 14-16 Jan.,1988.